Iranian Journal of Science and Technology, Transactions of Civil Engineering (2023) 47:1845–1860
https://doi.org/10.1007/s40996-022-01014-5

RESEARCH PAPER

Model Test on Flow Field Characteristics of the Combined Complementary Double-Hole Network Ventilation with Shaft

Shuai Yang[1] · Ya-Qiong Wang[1,2] · Ya Xiong[3] · Yun-Xiao Xin[4] · Min Deng[5] · Yan-Jie Hu[5] · Rui Ren[1]

Received: 24 August 2022 / Accepted: 29 November 2022 / Published online: 8 December 2022

Abstract

The ventilation system significantly influences tunnel operation safety, energy savings, and reduced consumption. The Ying'erling highway tunnel proposed a hybrid ventilation system combined with complementary double-hole network ventilation with a shaft. A ventilation model test platform was designed based on similarity theory with a 1/10 transverse length scale. The test platform was used to study the flow field distribution in the hybrid ventilation system under different shaft supply and exhaust conditions. The test results determined the wind speed and pressure distribution at measurement sites in the uphill and downhill tunnel and obtained the influence law of the shaft in the supply and exhaust state on the flow field distribution. A field test of the ventilation performance during tunnel operation showed that the trend of model test results is the same as that of field test results, which verifies the reliability of the test platform. The test results were used to optimize the ventilation control of the Ying'erling tunnel. The study provides an essential guide for the ventilation system design of a long highway tunnel.

Keywords Tunnel engineering · Mixed ventilation system · Physical model experiment · Field test · Flow field characteristics

1 Introduction

China's highway tunnel construction has developed recently, and energy consumption during tunnel operation has increased. Therefore, choosing a suitable ventilation system for tunnel design is essential. An appropriate ventilation system can improve ventilation efficiency and save costs to meet the ventilation requirements. For the current tunnel ventilation system, vertical shaft sectional ventilation is frequently used in the long tunnel (Ji et al., 2013; Guo et al., 2018, Wan et al., 2019). Because of this, the ventilation system satisfied the requirement of air volume and the requirement of smoke exhaust distance. Qinlingzhongnanshan highway tunnel is the second-longest tunnel globally, with a total length of 18.02km. The tunnel was ventilated by being divided into sections (Xie et al., 2013); it can meet the air requirement of each area and ensure that the wind speed will not exceed the allowable wind speed. The successful application of a longitudinal ventilation system in the Zhongnanshan tunnel has promoted the construction of a super-long tunnel in China. Applied Large Eddy Simulation (LES) method, Ji et al. (2013) studied the influence of cross-sectional area and aspect ratio of the shaft on natural ventilation. In conclusion, the shaft with a larger cross-sectional aspect ratio should be divided into several smaller shafts to better the smoke exhaust effect. Zhang et al. (2018) decreased the Yunshan tunnel's energy consumption and maintenance costs by optimizing the shaft's diameter and position and reducing the number of jet fans in the original ventilation system. In CFD numerical simulation, Xie et al. (2018) studied the influence of cross-sectional area and aspect ratio of the shaft of natural smoke exhaust in a tunnel fire. Guo et al. (2018) constructed a reduced-scale (1:10) tunnel with four shafts

✉ Rui Ren
renrui@chd.edu.cn

1 School of Highway, Chang'an University, Xi'an 710064, China

2 Shaanxi Provincial Major Laboratory for Highway Bridge and Tunnel, Xi'an 710064, China

3 Chongqing Communications Planning Survey and Design Institute, Chongqing, China

4 Nanjing University, Nanjing 210093, China

5 CCCC Second Highway Consultants Co. Ltd, Wuhan 430056, Hubei, China

to investigate the fire smoke propagation in the tunnel. Peng and Shi (2019) put forward the basic idea and method of a shaft design for a super-long highway tunnel based on the Xianrendong tunnel.

In the longitudinal ventilation system, the limit length of ventilation is 3km. When it exceeds 3km, it is necessary to add appropriate auxiliary channels or fans to meet the requirements. Therefore, this increased the ventilation system's initial investment and operation energy consumption (Huang and Pan, 2011; Hu et al., 2011). Many scholars have conducted several studies to reduce energy consumption, and several shafts solved the problem of long ventilation distances. Bener and Day (1991) presented the idea of "twin-tube complementary ventilation." This conception solves the imbalance problem between the uphill and downhill tunnels regards the twin-tube tunnel as a unit rather than two separate tunnels. Zhang, Lei, and Tian (2011a, b) put forward the concept of air exchange mode and analyzed its application and design algorithm. This method uses the cross-passage exchange of the air to meet the air quality requirements of the two tunnels. The idea of "two-tube complementary" and the "air exchange mode" proposal had attracted wide attention.

In 2011, twin-tube complementary longitudinal ventilation was applied in the Dabieshan tunnel for the first time worldwide. Researchers began to analyze the characteristics of complementary ventilation using different methods, such as ventilation mode, volume, scope, and economic level (Hu et al., 2011; Zhang et al., 2011a, b). Wang et al. (2014a, b) analyzed the test data through the field test and found the function and existing problems of air interchange cross-passage under the twin-tube complementary ventilation system. Adopted the finite element simulation analysis method, Ren et al. (2018) studied the effectiveness and influencing factors of the complementary ventilation system concerning particulate matter concentration distribution. Based on the compensation principle and optimization theory, Chai et al. (2018, 2019) proposed the energy-saving optimization mode of tunnel air supplement design based on the compensation concept, which provides a reference for the energy-saving design of the long-distance highway tunnel ventilation system. Wang et al. (2014a, b, 2020a, b, c) and Xia et al. (2015) established a scale model based on the similarity theory to verify the feasibility and reliability of the complementary ventilation mode. Complementary ventilation has the advantages of low energy consumption, more reasonable pollutant concentration distribution, and high visibility. However, for the tunnel over 5km, this ventilation system will lead to excessive downhill wind speed and can't meet the smoke exhaust requirements. At the same time, a complementary ventilation system can't meet the air volume demand in the tunnel operation's later stage. As a result, long tunnels under construction have superior longitudinal ventilation through comparison and selection (Wang et al., 2019a, b, Zhou et al., 2020) rather than complementary ventilation. Suppose we can fully play the advantages of a complementary ventilation system in the long tunnel, which requires setting up shafts for ventilation in different sections. In that case, it will obtain more significant economic benefits (wang et al., 2020a, b, c). With the increase in traffic volume and tunnel mileage, the air demand of the tunnel increases significantly, and the twin-tube complementary ventilation system cannot meet the requirements. If segmented longitudinal ventilation and double-hole complementary ventilation can be combined to give full play to their advantages, more significant economic benefits will be obtained (Wang et al., 2020a, b, c). This new mixed ventilation system, combined with complementary ventilation with the shaft, was adopted in the Ying'erling tunnel. At present, there is little research on this hybrid ventilation system.

The subject of this study is the flow field characteristics of hybrid ventilation systems in Ying'erling's long road tunnel on the Rongwu Expressway. A scale model test platform based on similarity theory was designed and built to simulate ventilation in the tunnel. The test platform simulated the hybrid ventilation system combined with complementary ventilation with the shaft supply and exhaust. A field ventilation test was conducted to investigate the platform's reliability. Two axial fans at the complementary cross-passage of the tunnel were used to drive the uphill and downhill tunnels for gas exchange. The axial-flow fan of the shaft adjusts the wind speed through the frequency converter to simulate the air supply and exhaust state, and its influence on the wind speed and wind pressure at different positions in the tunnel is studied. Suggest corresponding ventilation control according to the flow field distribution in the tunnel. The paper can be used as a reference for the ventilation design of long tunnels.

2 Engineering Background and Ventilation System Comparison

2.1 Engineering Background

The Ying'erling tunnel in Hebei Province, China, was intended to be a separated twin-tube one-way three-lane tunnel. The tunnel is located in the Taihang Mountains, where the fault fracture zone of soft surrounding rock changes frequently, and the terrain and geology are complex. It is the control project of the Rongcheng–Wuhai Expressway. The location of the tunnel is shown in Fig. 1.

The Ying'erling tunnel is a twin-tube tunnel, and the distance between the two tunnels is 30 m. The left tunnel (i.e., downhill tunnel) is 5656 m long, with slopes of −2.15%. The right (i.e., uphill) is 5677 m long, with a gradient of +2.15%. The designed speed limit is 100 km/h for a Class

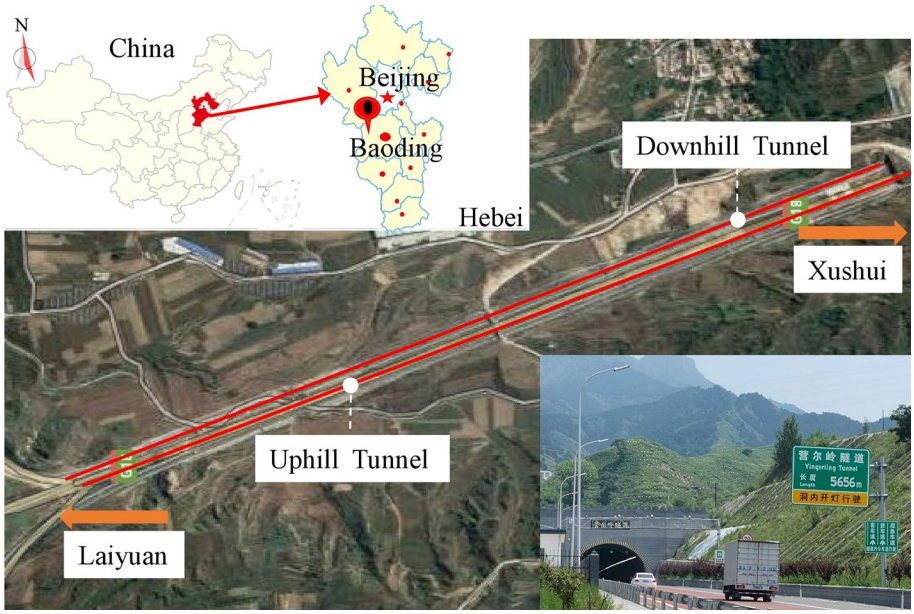

Fig. 1 Locations of Ying'erling tunnel

I highway. The maximum depth of the tunnel is about 482 m. The average altitude is 1000 m, and the cross-area is 99.47 m^2. The whole tunnel is a one-way longitudinal slope, and the increase of pollutant concentration in the tunnel is approximately proportional to the longitudinal length of the tunnel. The main engineering parameters of the Ying'erling tunnel are shown in Table 1.

2.2 Ventilation System

The long-term air demand of the right tunnel is 1092 m^3/s, and the left is 465.54 m^3/s. The air demand of the two tunnels varies greatly, with a ratio of 2.35. The wind speed in the right line tunnel exceeds 10 m/s. According to the engineering situation, a hybrid ventilation system combined with complementary ventilation with a shaft is proposed. As shown in Fig. 2, the hybrid ventilation system includes an uphill tunnel, downhill tunnel, air interchange cross-passage, ventilation shaft, etc. The hybrid ventilation system is based on longitudinal ventilation, and the tunnels are connected into a system through two air interchange cross-passages. The abundant fresh air uphill of the downhill tunnel is transported to the uphill tunnel through the air interchange cross-passage to increase the ventilation in the uphill tunnel. The dirty air of the uphill tunnel can transport to the downhill tunnel through the air interchange cross-passage to fully use the surplus air volume of the downhill tunnel to dilute the pollutants and reduce the contaminants at the wind speed in the uphill tunnel. According to the Ying'erling tunnel's air demand characteristics and the disaster prevention and rescue requirements, the complementary ventilation technology meets the daily operation ventilation. The smoke exhaust shaft meets the specification requirements.

Table 1 Main engineering parameters of Ying'erling tunnel

Item		Left tunnel	Right tunnel
Length (m)		5656	5677
Slope		-2.15%	+2.15%
Import and export stake No (m)		ZK99+535~ZK105+191	YK99+523~YK105+200
Average altitude (m)		1000	1000
Cross-area (m^2)		99.47	99.47
Equivalent diameter (m)		9.72	9.72
Forecast traffic volume	2025(Pcu/d)	52016	52016
	2035(Pcu/d)	63241	63241
Design traffic speed (km/h)		100	100
The average temperature of the tunnel site			
The temperature in summer (℃)		25	25

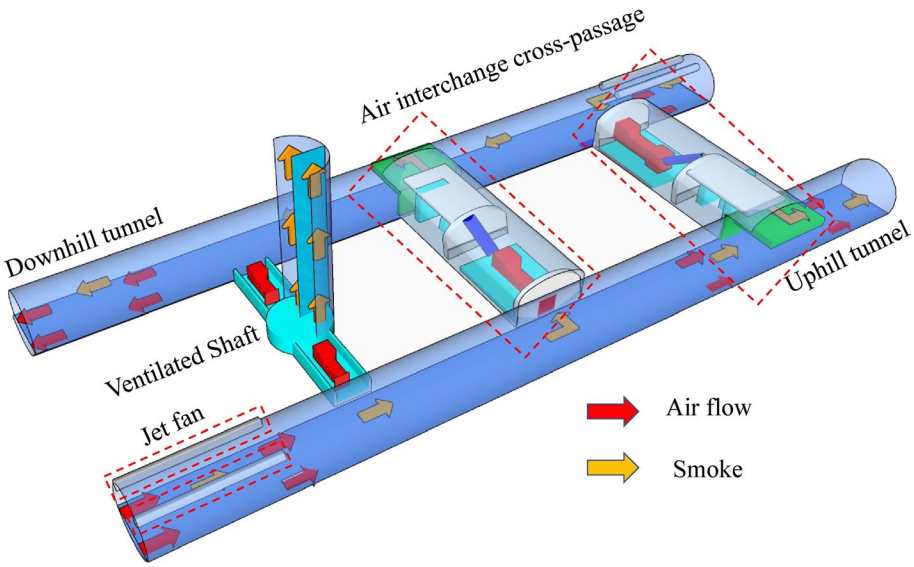

Fig. 2 Schematic of the mixed ventilation system

3 Physical Model Test System

3.1 Similarity Criteria and Model Scale

The hybrid ventilation system is made into a corresponding scale model to obtain the distribution law of wind speed and pressure in the tunnel during operation according to the similarity criteria (Roh et al., 2008; Lynde et al., 2019). Similarity theory is the theoretical basis of the model test. The following three aspects should be satisfied to ensure that a physical model of the ventilation system is similar to the actual tunnel, including geometric similarity, kinematic similarity, and dynamic similarity. The airflow in the tunnel can be regarded as the flow of incompressible viscous fluid (Pruitt et al., 2022). Therefore, the scaled ventilation model should have the Euler number E_u, Reynolds number R_e , and Strouhal number S_r similar to the prototype tunnel.

Reynolds number of prototype tunnel(Liu et al., 2020):

$$R_e = \frac{vD}{\upsilon} \tag{1}$$

where v denotes the air speed of the prototype tunnel, v=5.74m/s; D denotes the cross-sectional hydraulic diameter, $D = 9.72m$; υ denotes the coefficient of kinematic viscosity of air, υ=1.5 × $10^{-5}m^2/s$;$R_e = 8.37 \times 10^6$, and the airflow in the tunnel is turbulent flow at present.

The coefficient of frictional loss of prototype tunnel (Liu et al., 2020):

$$\lambda = \frac{1}{\left(2\lg\frac{3.7}{n}\right)^2} \tag{2}$$

Based on the Guideline for Design of Ventilation of Highway Tunnels, the value of λ is generally adopted 0.025 for the concrete-lined tunnels. Equation (2) is used to calculate the roughness $n = 0.0025$.

When the fluid reaches the self-modulation state (Wang et al., 2014a, b; Jin et al., 2015), the critical value R_{ec}:

$$R_{ec} = 4160\left(\frac{1}{2n}\right)^{0.85} \tag{3}$$

The value n is generally adopted as 0.0025. Equation (3) is used to calculate $R_{ec} = 3.75 \times 10^5$.

The airflow in the model is similar to the actual tunnel, which ensures the fluid in the model is in the self-modulation state rather than the equal Reynolds number. Therefore, let the Reynolds number of the model

$$R_{em} = \frac{R_e}{x_l \cdot x_v} \tag{4}$$

where x_l denotes the length ratio of the model to the actual tunnel; x_v denotes the time ratio of the model to the existing tunnel $x_v = 1$. When R_{em}>R_{ec}, the flow field of the model is in the self-modulation state. Equation (4) is used to calculate the value range x_l.

$$x_l < \frac{R_e}{R_{ec}} = \frac{8.37 \times 10^6}{3.75 \times 10^5} = 22.32 \tag{5}$$

Considering the deflection, test site, and technical feasibility, determining the model's scale is 1:10. The main section geometric dimensions of the prototype and model are shown in Table 2.

According to the scale, the test model of the Ying'erling tunnel should be 560m long. It is difficult to install a long tunnel model in the laboratory. Therefore, the model should be shortened from the two aspects of the economy and test operability. The resistance grid was added to the

Table 2 Design parameters of prototype and model

Parameters		Prototype	Model
General section	Height/m	9.83	0.983
	Width/m	10.91	1.091
	Area/m	99.47	0.995
	Equivalent diameter/m^2	9.72	0.972
Cross-passage section	Height/m	9.83	0.983
	Width/m	5.00	0.500
	Area/m	44.90	0.449
	Equivalent diameter/m^2	6.53	0.653

Fig. 3 Resistance grids

tunnel model's appropriate part, and the equivalent friction principle was used to replace the corresponding length. The equivalent model length of the resistance grid is (Lai, 2015):

$$L_{\mathrm{e}} = \frac{\lambda_m - 0.025}{0.025} L_j \tag{6}$$

where λ_m denotes the model resistance coefficient after adding resistance grid; L_j denotes the model length between resistance grid, m.

The model is made of Plexiglas, and the resistance coefficient after adding the resistance grid $\lambda_m = 0.23$ is obtained through experimental measurements. As shown in Fig. 3, the resistance grid adopts 18 mesh wire mesh as the model resistance grid. The distance between two resistance grids exceeds three times the equivalent diameter. The distance between two resistance grids L_j is 3.6m in the model. According to Eq. (6), the equivalent model length L_e is 29.52m. The length of the test model was 79 m, and the total number of resistance grids required is $\frac{L-L_m}{L_e} = \frac{560-97}{29.52} = 16.29$. According to the calculation, it can be seen that 16 resistance grids should be installed in each tunnel. Since the position in the cross-passage is a sudden change in wind flow and needs to be monitored, two resistance grilles are subtracted from the corresponding position. Therefore, 14 resistance grilles are set in each tunnel, and 28 are placed in the model.

The scale model layout is shown in Fig. 4. The zone between two ventilation cross-passage is called short tracks, which are 10m long. The distance between the axes of the two main tunnels is 3m, and the axis of the main tunnel intersects the axis of the cross-passage vertically. The model and fan were fitted together through a flexible connection. The shaft can supply and exhaust air to two main tunnels through a Y-shaped structure. A stainless steel beam connected each model segment. A purple wool rope was attached to the top of the model to determine the wind direction of each section. Paste yellow and white stickers on the bottom of the model to show lane separation lines and curbs.

3.2 Power and Data Acquisition Systems

The ventilation system needs five fans, including three axial fans and two centrifugal fans. The model installed two SD64—11axial fans (as shown in Fig. 5a) in the air interchange cross-passage to satisfy the ventilation requirements in the model test. One SDS—112K axial fan (as shown in Fig. 5b) was set up in the Y-shaped shaft. The axial-flow fan was equipped with a frequency converter to control the air volume and wind speed in the model and study the airflow organization under different working conditions. Two centrifugal fans (as shown in Fig. 5c) were installed at the uphill and downhill tunnels entrance, respectively. The performance parameters of the axial fan are shown in Table 3, and a centrifugal fan is shown in Table 4.

The simulation process of the model test was dynamic, and the section wind speed and pressure were constantly changing. Therefore, timely and accurate data collection was of significant importance. Alpha Instruments' micro differential pressure sensor was selected to measure the wind pressure, with a measurement range of 0–250 Pa and a measurement accuracy of 1%. The STF30 wind speed sensor was selected, with a measurement range of 0–30 m/s and a measurement accuracy of ± 0.2 m/s, as shown in Fig. 6a. Measuring instruments were employed to convert air pressure into electrical signals. The converter can be related to the adjustment adapter through the shielded wire and then connected to the indicator to read the test data. The test element and adjustment adapter are shown in Fig. 6. The PCI 6224 data acquisition card launched by NI company in the USA and its supporting development platform LabVIEW are selected. The system realizes the input, data acquisition, real-time display, storage, playback, and result report output of the test system, which further ensures the reliability of

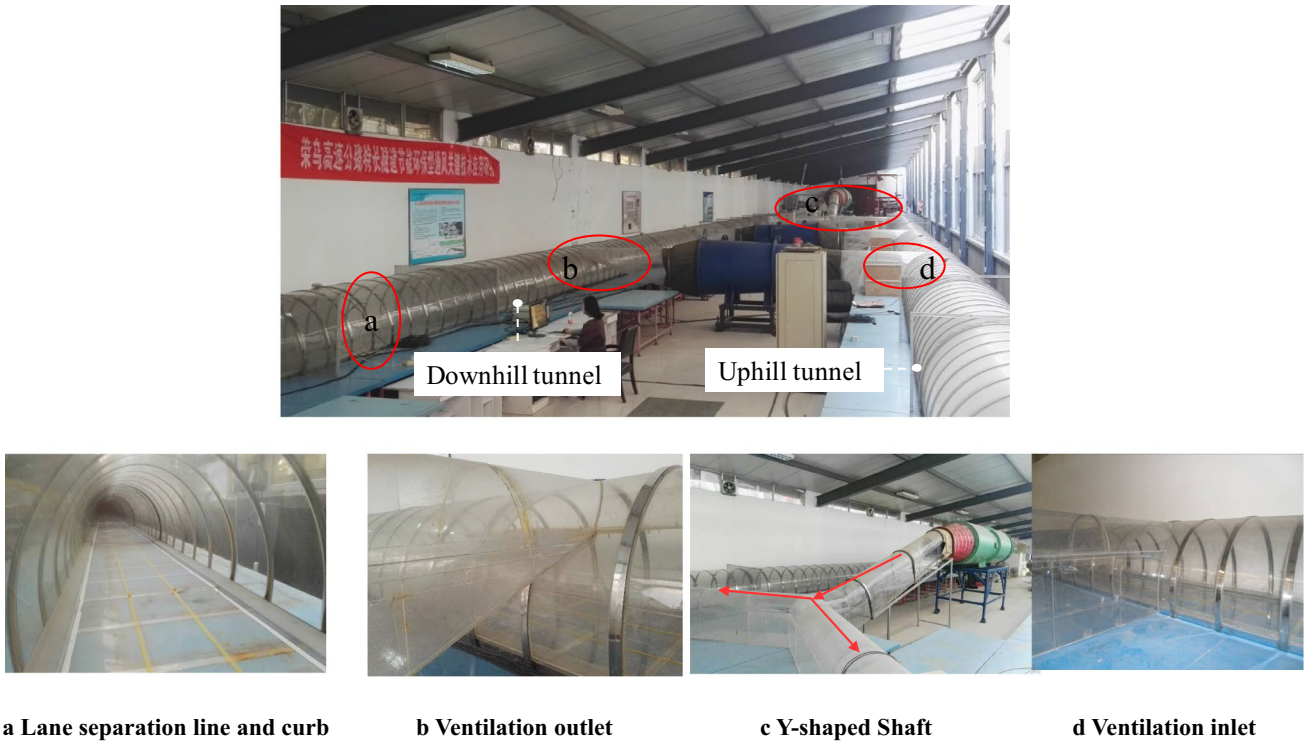

a Lane separation line and curb **b Ventilation outlet** **c Y-shaped Shaft** **d Ventilation inlet**

Fig. 4 Physical model platform

a. SD64—11axial fan **b. SDS—112K axial fan** **c. Centrifugal fan**

Fig. 5 The power system of a scale model for the Ying'erling tunnel

Table 3 Performance parameters of axial fan

Axial fan	Rotation speed (r/min)	Flow (m^3/h)	Total pressure (Pa)	Power (kW)	Internal efficiency (%)	Required power (kW)	Rationed power (kW)
SDS-112K	1480	82800	2200	–	–	30.3	37
SD64-11	1450	53120	1529	24.66	91.5	28.36	30

the test data. The system holds the characteristics of high efficiency and easy observation and analysis. Each section of data can be compared macroscopically in the test interface and displayed in the change curve of single data real-time monitoring. The system can manually set the time interval

Table 4 Performance parameters of centrifugal fan

Centrifugal fan	Rotation speed (r/min)	Thrust (N)	Flow (m^3/h)	Output speed (m/s)	Motor power (kW)	Sound pressure (dB)
L4-72S-6P-4	1450	919	3.2	14.2	4	61

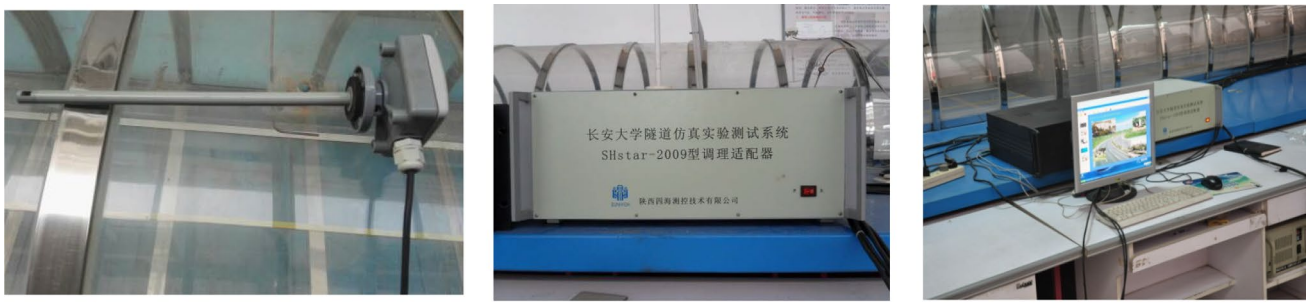

a. STF30 wind speed sensor **b. Adjustment adapter** **c. Data processing**

Fig. 6 Test system

of data collection and send out the alarm when abnormal data appears.

3.3 Test Scheme

Given the flow field distribution in the tunnel, the tunnel was divided into six parts. Figure 7 depicts the 10 test sections in the test model. Sections 1# to 5# were located at the tunnel inlet, ventilation section, short track, air supply section, and outlet of the uphill tunnel, respectively. Conversely, test sections 6# to 10# locate at the tunnel outlet, air supply section, short track, ventilation section, and the inlet of the left tunnel, respectively. Two wind pressure gauges and one anemometer were installed at each test section. Figure 8 shows the arrangement of measuring points for wind speed and pressure.

The experiment was divided into four operating conditions: the uphill tunnel shaft air supply, the downhill tunnel shaft air supply, the uphill tunnel shaft air exhaust, and the downhill tunnel shaft air exhaust. Throughout the model test, the 2# and 3#fan frequency remains unchanged at 25 Hz, and set the 5# fan as different values, including 20 Hz, 25 Hz, 30 Hz, 35 Hz, 40 Hz, and 45 Hz. That is 25 combinations of working conditions in total. The airflow is fully developed after the 30s of fan frequency adjustment. The airflow was measured at every section in the test model for

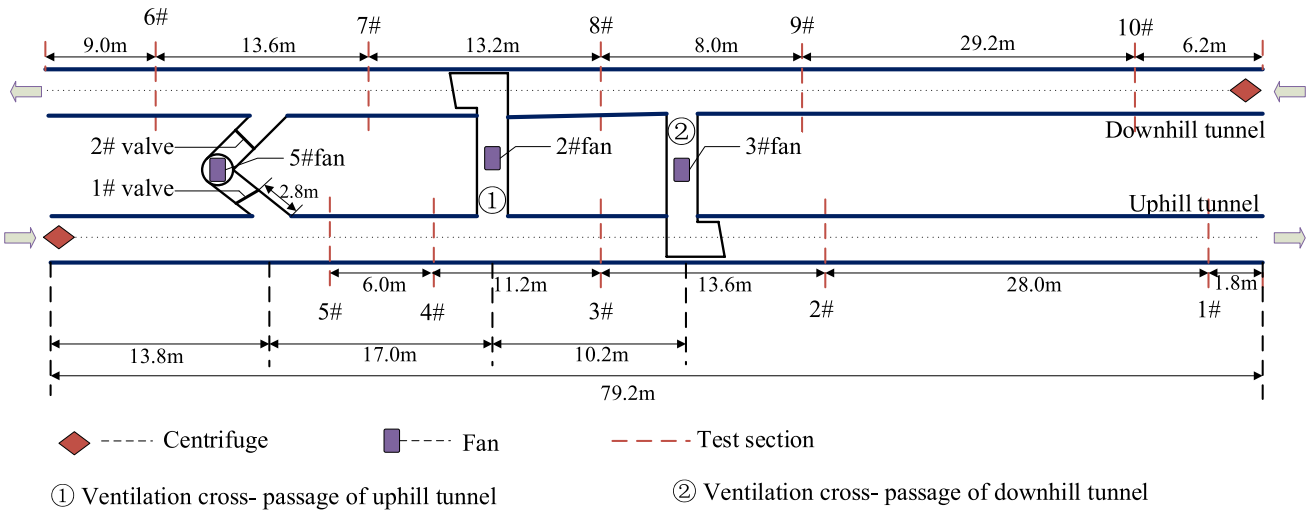

Fig. 7 Tunnel partition

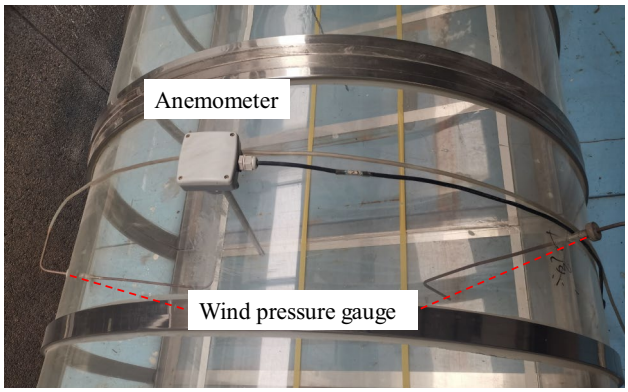

Fig. 8 Test section

every working condition. The measurement parameters include wind speed and wind pressure at every test section. The specific data of each state were compared and analyzed.

3.4 Field Measurement Verified the Reliability of the Model

Field measurements of the Ying'erling tunnel were conducted (Liu et al., 2020; He et al., 2020) to ensure the accuracy of the scale model platform. Due to the complex situation on-site during the operation period, the staff of the expressway management office opened two axial-flow fans in the ventilation cross-passage for on-site detection. Therefore, the data collected by the physical experiment platform under the same working conditions (complementary ventilation mode) are compared with the field test data to verify the reliability of the model platform.

3.4.1 Field Test Equipment

A KESTREL high-precision anemometer and an AR866A anemometer were used for the field test, as shown in Fig. 9a. The KESTREL anemometer has the advantages of high sensitivity, high precision, easy operation, and recording. The range is 0.6~60 m/s, the accuracy is 3%, and the resolution is 1 m/s. Although this hand-held anemometer has high accuracy, it cannot measure wind speed over 2m in height. For height of more than 2 m used the AR866A anemometer to measure the wind speed with the telescopic rod of the level, as shown in Fig. 9b and c. The anemometer was tied to the telescopic rod, and the design height of the test point was achieved by adjusting the telescopic rod. The wind speed sensor is connected to the display through the induction line to read data at the low position. The range of the AR866A anemometer is 0~30m/s, accuracy±5%, and the resolution is 0.01 m/s.

3.4.2 Field Test Scheme

During the field test, open the axial-flow fan of the ventilation cross-passage and the exhaust fan of the uphill shaft, and the air volume in the main tunnel was 900 m^3/s. Measurements are taken from 10 a.m. to 12 p.m. and from 4 p.m. to 6 p.m. The emergency parking lane on the right side of the tunnel was closed to ensure the testing effect and safety. Therefore, the test site used the emergency parking lane and above the side ditch. Five test sections were set at the characteristic positions of the uphill and downhill tunnels, respectively. As shown in Fig. 10, set nine test points on the test section, 1 m, 2.5 m, and 4.0 m high from the carriageway. The average wind speed of the nine test points was regarded

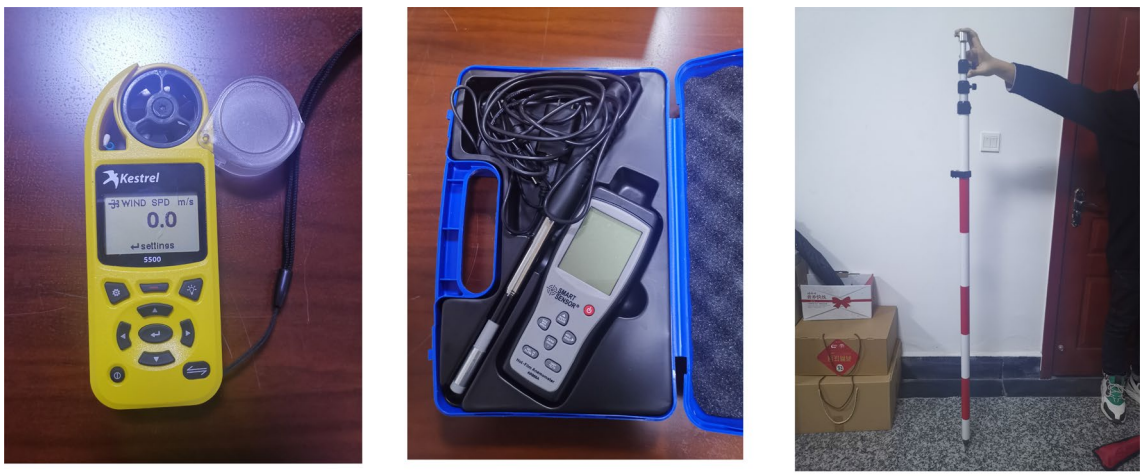

a KESTREL anemometer b AR866A anemometer c Telescopic rod with level

Fig. 9 Test equipment

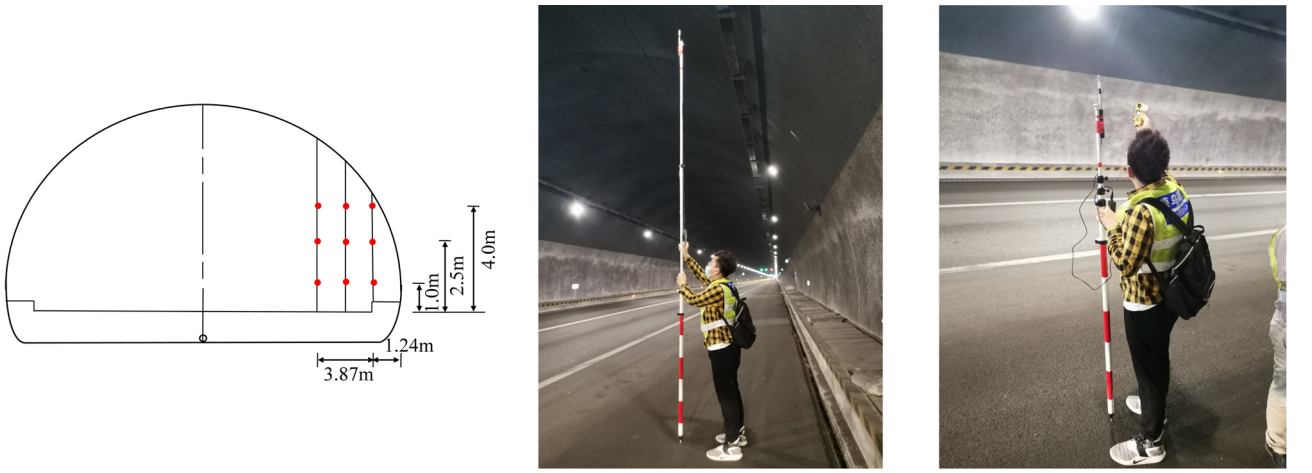

a. Test point layout

b. Wind speed measurement at high altitude

c. Wind speed measurement at low altitude

Fig. 10 Test point layout and field measurement

as the wind speed measurement value of the test section, and the field test is shown in Fig. 9b and c. The wind speed measuring points of the actual tunnel reflect the longitudinal distribution trend of wind speed. Five landmark test sections were selected for the uphill and downhill tunnels, respectively. The location is as follows: set one test section between the tunnel entrance and the ventilation cross-passage; set one test section in the middle of two ventilation cross-passages; set one test section between the ventilation cross-passage and the shaft; set two test sections between the shaft and the outlet. The stake numbers of these test sections in the uphill tunnel are YK981+343, YK981+408, YK981+548, YK982+793, YK983+375, and the downhill tunnel are ZK981+345, ZK981+420, ZK981+540, ZK982+805, ZK983+366.

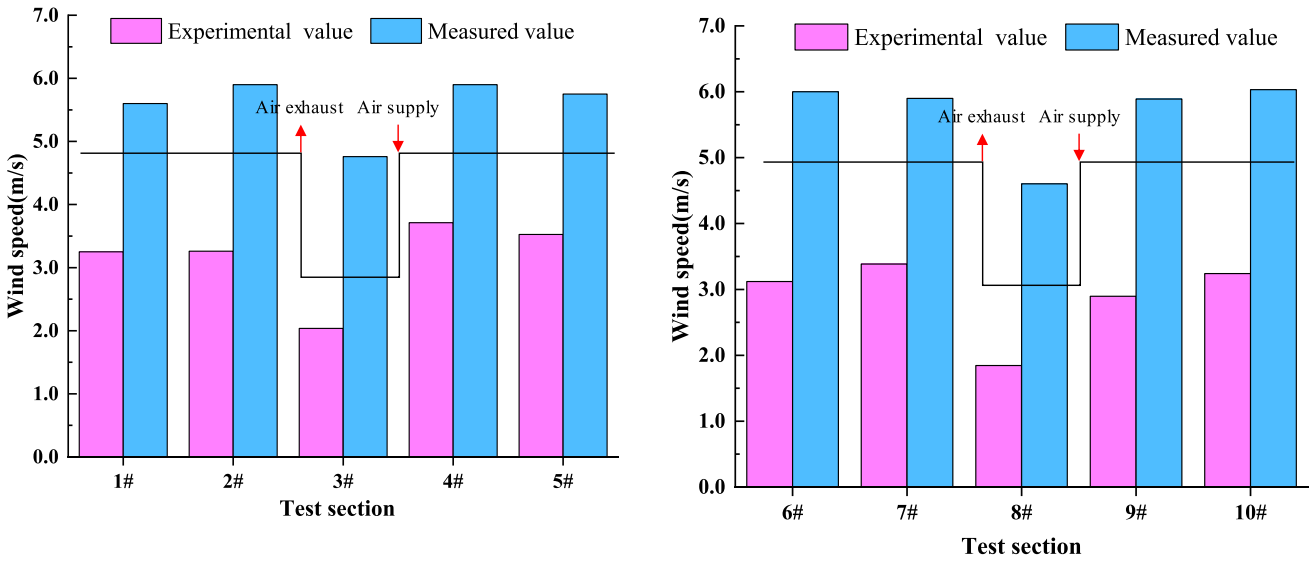

a. Comparison of the uphill tunnel

b. Comparison of the downhill tunnel

Fig. 11 Data comparison

3.4.3 Field Test Results and Validation Analysis

Figure 11 compares experimental and measured wind speed values at the characteristic positions of the uphill and downhill tunnels. The experimental value is lower than the measured value. Due to the limitation of laboratory conditions, the fan frequency used in the physical experiment is lower than the axial fan frequency in the actual tunnel. The power of the axial fan in the cross-passage in the Ying'erling tunnel is 70kw, and the axial fan's power in the model's cross-passage is 30kw. It is also possible that the wind speed at the measurement point is low due to the influence of the resistance grid. As shown in Fig. 11, the variation trend of the experimental value and the measured value of the uphill and downhill tunnel is the same, and the wind speed is the lowest in the middle of the two ventilation cross-passages. This is the same trend as the wind speed variation of the delivery and exhaust combination in the Guideline for Design of Ventilation of Highway Tunnels. (The black line in Fig. 11 represents the wind speed trend under the combination of supply and exhaust, independent of the value.) The wind speed of the 2#-3# section decreases due to the exhaust from the uphill tunnel to the downhill tunnel. As the downhill tunnel supplied air to the uphill tunnel, the 3#-4# section wind speed increased. The wind speed of the 9#-8# section decreases due to the exhaust from the downhill tunnel to the uphill tunnel. As the uphill tunnel supplied air, the downhill tunnel, the 8#-7# section wind speed increased. Therefore, the experimental results of the scale model were reliable.

4 Results Analysis

Before the formal test, adjust the fan to the preset working state through the frequency converter, which takes about 1 min. According to the test results exported by the PCI 6224 data acquisition system, the wind speed and pressure tends to be stable 10 s after the fan frequency conversion adjustment. Therefore, set the data acquisition interval to 20 s. The airflow in the tunnel model has been fully developed and can accurately show the flow field distribution after working conditions change. Each working condition was tested three times, and used the average value of the three experiments was for data processing.

4.1 Uphill Tunnel Shaft Air Supply

In tunnel operation, the shaft supplies air to the uphill tunnel. Opened the 2# shaft valve and air supply and set the 2#fan and 3# fan frequency as 25 Hz. Meanwhile, put the 5#fan as different works, including 20, 25, 30, 35, 40, and 45 Hz. The 5# fan was adjusted to the preset working condition through the frequency converter, waiting for the 20 s for the airflow to stabilize and then extracting the data. The test results are shown in Fig. 12.

As shown in Fig. 12a, the wind speed increases first, decreases, and gradually increases following the travel direction. Figure 12b shows that the wind speed increases first and then decreases, then rises slowly, and finally falls following the direction of travel. Under the operation of the 2# fan in the ① air interchange cross-passage, the wind speed from 4# to 3# section rapidly decreases from 3.49m/s to 1.43m/s, and the wind speed from 8# to 7# section increases sharply, indicating that the airflow in the uphill tunnel has entered the downhill tunnel. Under the operation of the 3# fan in the ② air interchange cross-passage, the wind speed from 9# to 8# section rapidly decreases, and the wind speed from 3# to 2# section increases sharply, indicating that the airflow in the downhill tunnel has entered the uphill tunnel (Wang et al., 2020a, b, c). Due to the air supply from the shaft, the wind speed from 5# to 4# section increases dramatically to 3.49 m/s, which conforms to the wind speed distribution given in the Guidelines for Design of Ventilation of Highway Tunnels (JTG/T D70/2-02-2014) (Ministry of Transport of the People's Republic of China, 2014) for a tunnel under the shaft longitudinal ventilation mode. The wind speed of the 7-10# test section in the downhill tunnel decreases with the increase of 5# fan frequency, and the wind speed of the 6# test section decreases with the increase of 5# fan frequency.

Figure 12c shows that the uphill tunnel's pressure rises and falls following the travel direction. Figure 12d shows that the pressure of the downhill tunnel increases first and then tends to be stable, then increases, and finally decreases. The pressure in the downhill tunnel increases with the 5# fan frequency increase. Uphill tunnel air supply plays the role of supplementing air volume and ventilation power. The effect is most obvious in the downhill tunnel, especially near the 7# section, which is conducive to the airflow of the uphill tunnel entering the downhill tunnel through the ① cross-passage. The air exhaust section of the uphill tunnel to the ① cross-passage and then to the air supply section of the downhill tunnel is one air path. Therefore, the direct effect of the uphill tunnel shaft air supply is to increase the pre-rise pressure in the downhill tunnel and therefore has a greater impact on the downhill tunnel.

4.2 Downhill Tunnel Shaft Air Supply

In tunnel operation, the shaft supplies air to the downhill tunnel. Opened the 1# shaft valve and air supply and set the 2#fan and3#fan frequency as 25 Hz. Meanwhile, set the 5#fan as different works, including 20, 25, 30, 35, 40, and 45 Hz. The 5# fan was adjusted to the preset working condition through the frequency converter, waiting for the 20s for

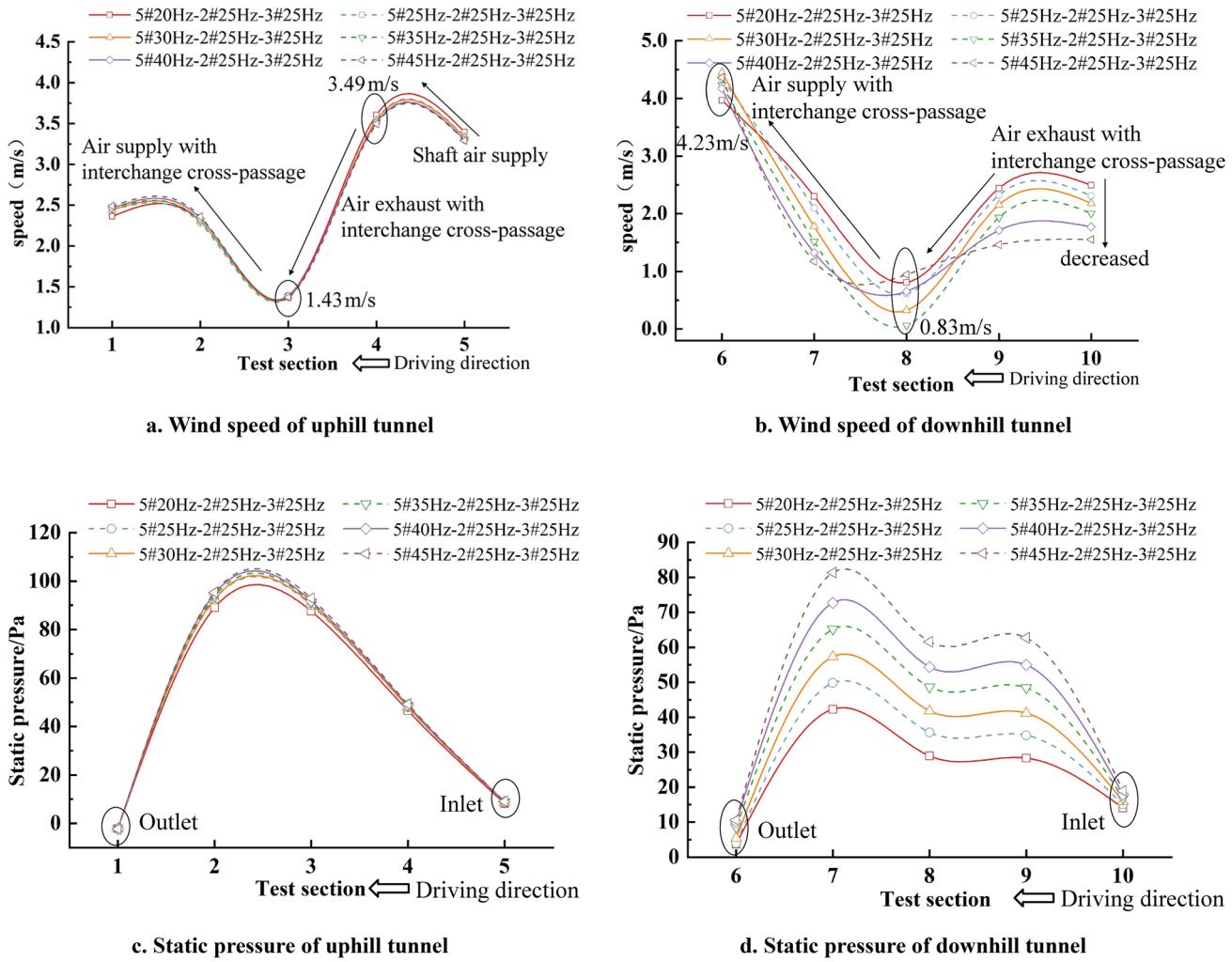

a. Wind speed of uphill tunnel

b. Wind speed of downhill tunnel

c. Static pressure of uphill tunnel

d. Static pressure of downhill tunnel

Fig. 12 Wind speed and static pressure

the airflow to stabilize and then extracting the data. The test results are shown in Fig. 13.

As shown in Fig. 13a, the wind speed trend increases first, decreases, and decreases along the direction of travel. Figure 13b shows that the wind speed increases slightly and then decreases suddenly, then rises again and decreases along the travel direction. In the complementary ventilation section, the decrease of wind speed at 4#-3# section and 9#-8# section corresponds to the increase of wind speed at 8#-7# section of the downhill tunnel and 3#-2# section of the uphill tunnel. This phenomenon shows that complementary ventilation can effectively exchange gas between the two tunnels (Wang et al., 2020a, b, c). Due to the air supply from the shaft, the wind speed from 6# to 7# section increases, which conforms to the wind speed distribution given in the Guidelines for Design of Ventilation of Highway Tunnels (JTG/T D70/2-02-2014) (Ministry of Transport of the People's Republic of China, 2014) for a tunnel under the shaft longitudinal ventilation mode. With the rise in the frequency of 5#fan, the wind speed of the uphill tunnel increased.

Figure 13c shows that the uphill tunnel's pressure rises and falls following the travel direction. Figure 12d shows that the pressure of the downhill tunnel increases first, increases, decreases, decreases, and decreases slowly. With the rise in the frequency of 5#fan, the pressure of the uphill tunnel increased. Downhill tunnel air supply supplements air volume and the effect is most apparent in the uphill tunnel. Meanwhile, the 7# section of the downhill tunnel is pressurized and reaches 31.22 Pa. With the increase of 5#fans, the wind speed and pressure of the uphill tunnel increase, which is conducive to the flow in the uphill tunnel and the gas exchange from the uphill tunnel to the downhill tunnel. The uphill tunnel shaft air supply and the pre-rise pressure

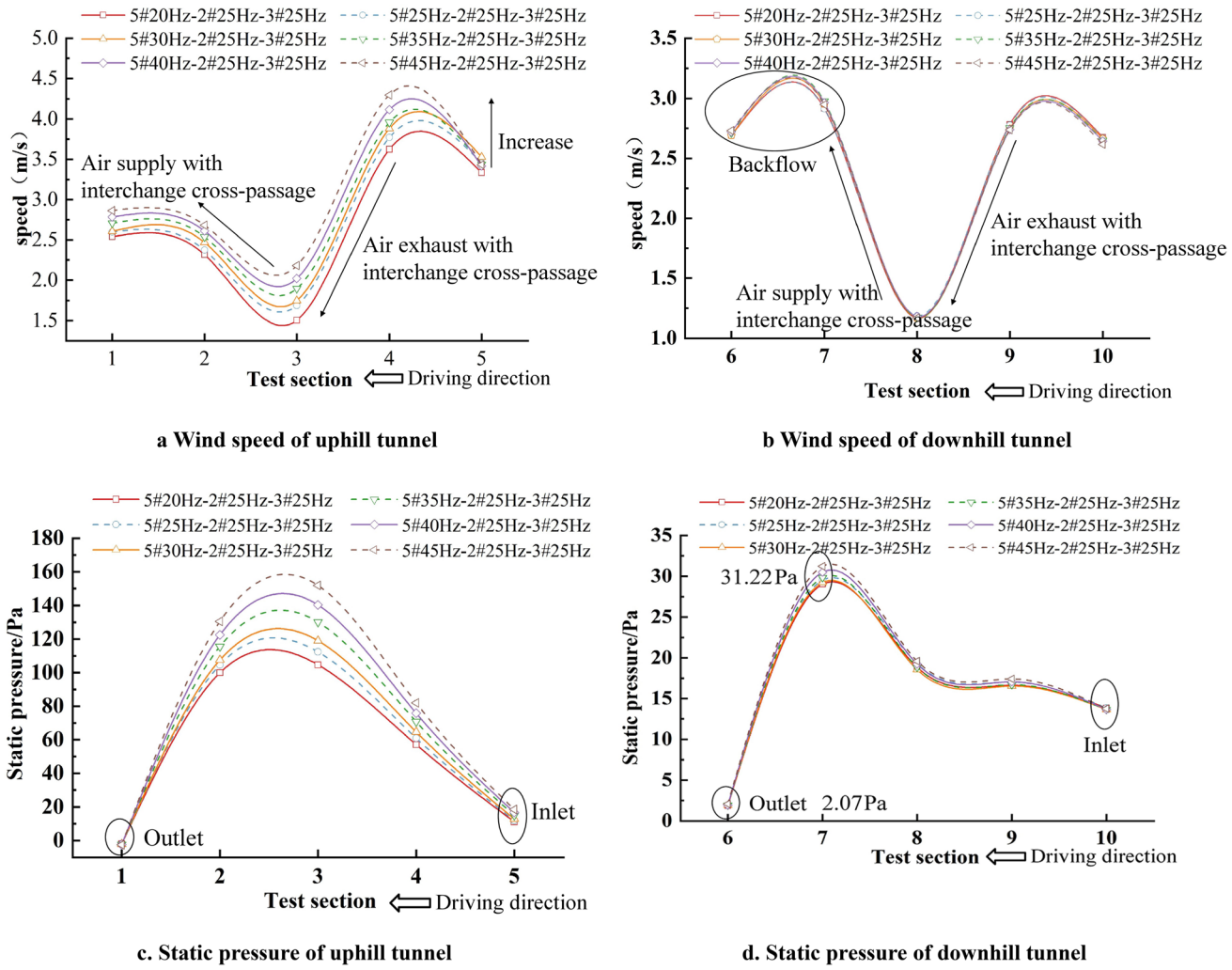

Fig. 13 Wind speed and static pressure

of the air path through the ① cross-passage increases, which increases the ventilation power of the uphill tunnel exhaust section and therefore has a more pronounced effect on the uphill tunnel.

4.3 Uphill Tunnel Shaft Air Exhaust

In tunnel operation, the uphill tunnel shaft exhausts air through the shaft. Opened the 2# shaft valve and air exhaust and set the 2#fan and 3# fan frequency as 25Hz. Meanwhile, set the 5# fan as different works, including 20, 25, 30, 35, 40, and 45Hz. The 5#fan was adjusted to the preset working condition through the frequency converter, waiting for the 20s for the airflow to stabilize and then extracting the data. The test results are shown in Fig. 14.

As shown in Fig. 14a, the trend of wind speed increases first and then decreases along the direction of travel Fig. 14b shows that the wind speed increases slightly and then decreases suddenly, then rises again and finally falls along the direction of travel. In the complementary ventilation section, the distribution law of airflow is the same as that studied above (Wang et al., 2020a, b, c). As the shaft is close to the entrance section of the uphill tunnel, the exhaust is beneficial for the flow field flow in the entrance section, and the 5#-4# section wind speed is high. With the 5# fan frequency increase, the wind speed of uphill and downhill tunnels does not change significantly. The wind speed at the 6# section varies obviously, likely caused by the operation error.

Figure 14c shows that the pressure of the uphill tunnel first rises and then falls following the travel direction. Figure 14d shows that the pressure of the downhill tunnel

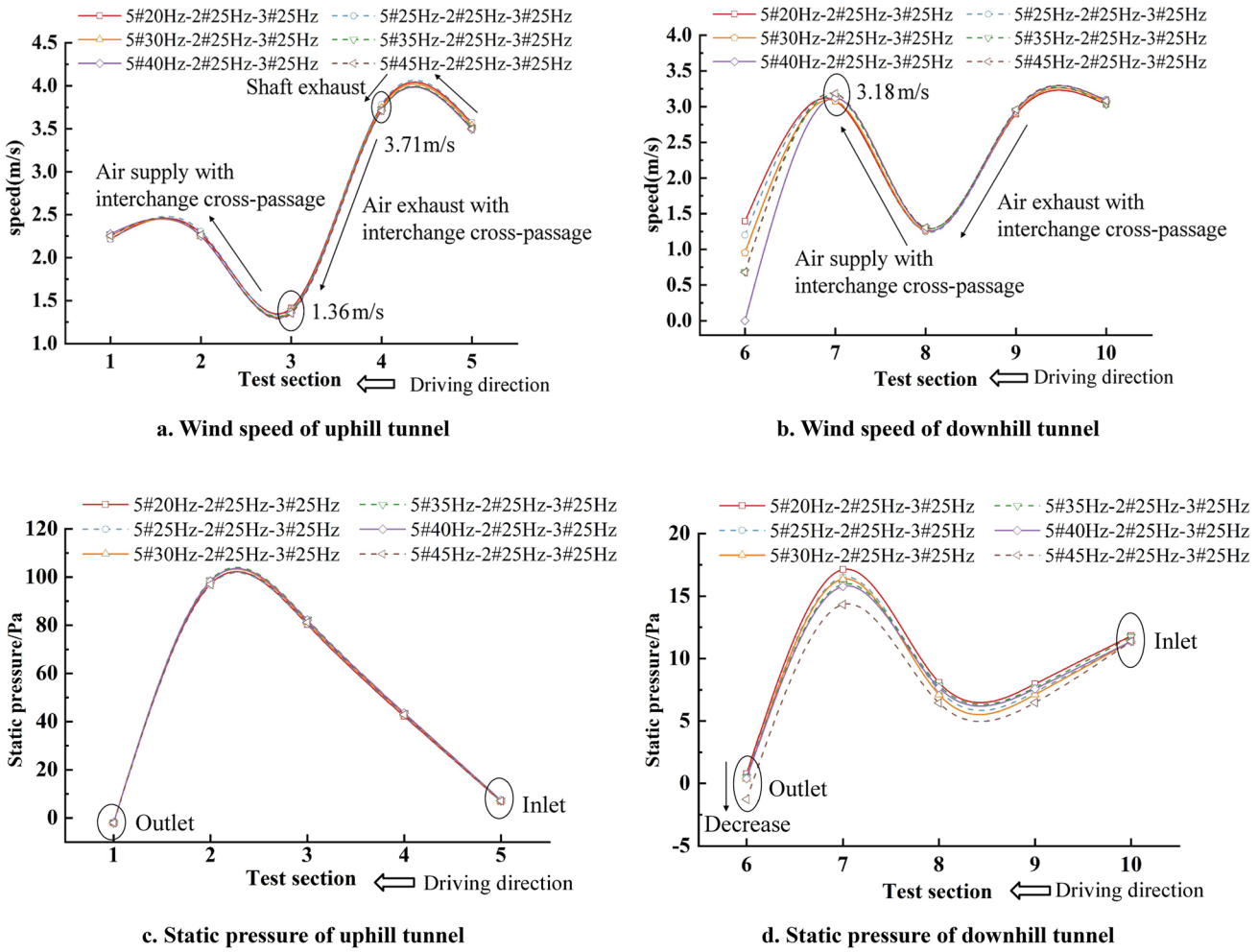

a. Wind speed of uphill tunnel

b. Wind speed of downhill tunnel

c. Static pressure of uphill tunnel

d. Static pressure of downhill tunnel

Fig. 14 Wind speed and static pressure

decreases first, then increases, and then decreases. With the rise in the frequency of 5#fan, the pressure of the downhill tunnel decreased. The uphill tunnel air exhaust reduces the air volume in the tunnel, which conforms to the rule given in the Guidelines for Design of Ventilation of Highway Tunnels (JTG/T D70/2-02-2014) (Ministry of Transport of the People's Republic of China, 2014) when the temperature difference inside and outside the tunnel is large in winter. Overall, the uphill shaft exhaust significantly impacts the air volume and static pressure downhill tunnel more than in the uphill tunnel. The uphill tunnel shaft exhaust and the pre-rise pressure of the air path through the ① cross-passage are reduced, increasing the ventilation power of the downhill tunnel exhaust section and having a more pronounced effect on the downhill tunnel.

4.4 Downhill Tunnel Shaft Air Exhaust

In tunnel operation, the downhill tunnel shaft exhausts air through the shaft. Opened the1# shaft valve and air exhaust and set the 2#fan and 3#fan frequency as 25 Hz. Meanwhile, put the5#fan as different works, including 20, 25, 30, 35, 40, and 45 Hz. The 5#fan was adjusted to the preset working condition through the frequency converter, waiting for the 20s for the airflow to stabilize and then extracting the data. The test results are shown in Fig.15.

As shown in Fig. 15a, the wind speed trend increases first and then decreases along the travel direction. (Fig. 15b shows that the wind speed drops first, rises, and finally falls following the travel direction.) In the complementary ventilation section, the distribution law of airflow is the same as that studied above (Wang et al., 2020a, b, c). The wind speed of 7# to 6#section decreases due to shaft exhaust. As

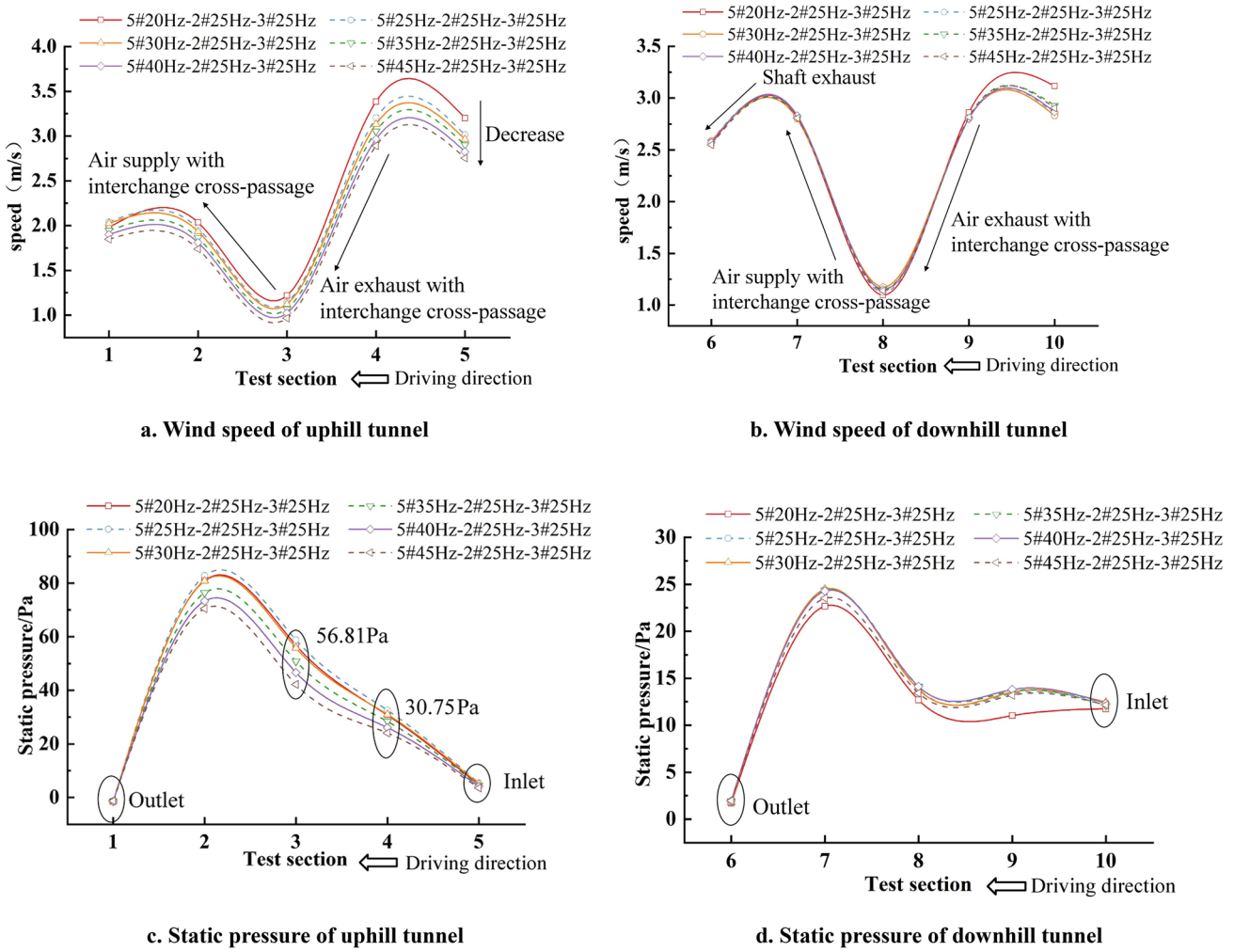

a. Wind speed of uphill tunnel

b. Wind speed of downhill tunnel

c. Static pressure of uphill tunnel

d. Static pressure of downhill tunnel

Fig. 15 Wind speed and static pressure

the shaft is close to the exit section of the downhill tunnel, it is conducive to the discharge of polluted airflow in the prototype tunnel. With the increase of 5#fan frequency, the wind speed of the uphill tunnel decreases, while that of the downhill tunnel does not change significantly.

Figure 15c shows that the pressure of the uphill tunnel first rises and then falls following the travel direction. Figure 15d shows that the pressure of the downhill tunnel remains stable, then increases and decreases. With the rise in the frequency of 5#fan, the pressure of the uphill tunnel decreased. The shaft exhaust at the exit of the downhill tunnel plays the role of diversion air and is conducive to gas exchange from the uphill tunnel to the downhill tunnel. It conforms to the rule given in the Guidelines for Design of Ventilation of Highway Tunnels (JTG/T D70/2-02-2014) (Ministry of Transport of the People's Republic of China, 2014) for a tunnel under longitudinal ventilation mode of shaft exhaust. The downhill tunnel shaft exhaust, which also increases the ventilation power of the air path through the ① cross-passage, has a more pronounced impact on the uphill tunnel.

5 Conclusion

A 1/10 (transverse length scale) model test platform was designed based on similarity theory and constructed to simulate ventilation in the Ying'erling tunnel. We used the system to simulate physical tests for tunnels with complementary double-hole network ventilation and shaft ventilation systems and provide an essential means of optimizing the design of ventilation systems for long tunnels. The field measurement verifies the reliability of the model test platform. The hybrid ventilation system proposed in this paper solves the problem of the limited applicable length of the complementary double-hole network ventilation. It provides a new idea for selecting ventilation methods for long tunnels

with slopes. The results of the study provide a reference for ventilation design.

(1) In the complementary ventilation section, the high-concentration pollutants uphill have transported downhill, and fresh air from the downhill is supplemented to the uphill tunnel, which forms a U-shaped circulating ventilation section (Wang et al., 2014a, b, 2020a, b, c). The air supply and exhaust from the shaft cause the changes in wind speed and pressure on the tunnel, which was in agreement with the wind speed and pressure distribution for shaft air supply and air exhaust ventilation systems stipulated in the Guidelines for Design of Ventilation of Highway Tunnels (JTG/T D70/2-02-2014).
(2) Due to the limitation of laboratory conditions, the frequency of the laboratory fan is lower than that in the real tunnel, so the wind speed obtained in the laboratory is lower than the field-measured data. The variation trend of wind speed in the two conditions is the same, which verifies the reliability of the physical model.
(3) For the uphill tunnel, shaft air supply supplements air volume and ventilation power. For the actual downhill tunnel, shaft air supply supplements air volume, and the effect is more obvious in the uphill tunnel. Shaft air exhaust can diversion polluted air and is conducive to gas exchange from the uphill tunnel to the downhill tunnel. According to the flow field characteristic in the tunnel, flexible design of ventilation control mode to deal with different situations.

Acknowledgments The authors gratefully acknowledge the financial support for this work provided by the National Natural Science Foundation (No. 5197082676).

Data Availability The data used to support the findings of this study are available from the corresponding author upon request.

Declarations

Conflict of interest The authors declare that they have no conflicts of interest.

References

Baochao X, Yaxiong H, He H, Linna C, Yang Z, Chuangang F et al (2018) Numerical study of natural ventilation in urban shallow tunnels: impact of shaft cross section. Sustain Cities Soc 42:521–537

Bener MA, & Day JR (1991). A new concept for ventilation long twin-tube tunnels. In: Proceedings of the 7th international symposium on the aerodynamics and ventilation of vehicle tunnels. Cranfield, UK: BHR Group, 10,811–820

Chai L, Wang X, Han X, Song J, Lei P, Xia Y, & Wang Y (2018). Complementary ventilation design method for a highway twin-tunnel based on the compensation concept. Math Probl Eng 1-13

Chai L, Wang X, Han X, Xia Y, Wang Y, & Lei P (2019). Optimization method for twin-tunnel complementary ventilation design and its energy saving effect. Math Probl Eng. 1-19

Cong HY, Wang XS, Zhu P, Jiang TH, Shi XJ (2018) Experimental study of the influences of board size and position on smoke extraction efficiency by natural ventilation through a board-coupled shaft during tunnel fires. Appl Therm Eng 128:614–624

Fan CG, Ji J, Gao ZH, Han JY, Sun JH (2013) Experimental study of air entrainment mode with natural ventilation using shafts in road tunnel fires. Int J Heat Mass Transf 56(1–2):750–757

Guo Q, Zhu H, Yan Z, Zhang Y, Zhang Y, & Huang T (2018). Experimental studies on the gas temperature and smoke back-layering length of fires in a shallow urban road tunnel with large cross-sectional vertical shafts. Tunnel Undergr Space Technol

He X, Li A, Ning Y (2020) Optimization of outdoor design temperature for summer ventilation for undersea road tunnel using field measurement and statistics. Build Environ 167:106457

Hu YJ, Deng M, Yang T (2011) Application research for the complementary ventilation of Dabie mountains tunnel. Transp Sci Technol 2:56–59

Huang M, & Pan BY (2011). Research of ventilation design for highway tunnel. In: Proceedings of the international conference on management and service science. pp.1–3, Bangkok, Thailand

Ji J, Han JY, Fan CG, Gao ZH, Sun JH (2013) Influence of cross-sectional area and aspect ratio of Shaft on natural ventilation in urban road tunnel. Int J Heat Mass Transf 67:420–431

Jin S, Gong Y, Zhang G (2015) Flow field development and energy evolution in road tunnels with unidirectional uniform traffic. J Wind Eng Ind Aerodyn 147:44–76

JTG/T D70/2-02-2014. Guideline for design of ventilation of highway tunnels

Lai K (2015). Simulate research on the equivalent resistance of grid used to tunnel ventilation model test. Chang'an University

Li S, Liu X, Wang J, Fang G, Chen W, Deng S (2019) Reduced scale experimental study and CFD analysis on the resistance characteristic of utility tunnel's ventilation system. Energy Procedia 158:2756–2761

Liu K, Guo J, Wan L, Xu C (2020) A model test study to optimize the ventilation system of a long expressway tunnel. J Wind Eng Ind Aerodyn 207:104393

Lynde M N, Campbell R L, Viken S A. (2019). Additional findings from the common research model natural laminar flow wind tunnel test. In: AIAA Aviation 2019 Forum. 2019: 3292

Ministry of Transport of the People's Republic of China, 2014. Guidelines for design of ventilation of highway tunnels. China Communications Press Co., Ltd, Beijing (JTG/T D70/2-02), (in Chinese)

Peng JS, Shi JX (2019) Study on the shaft and inclined shaft scheme for the extra-large xianrendong tunnel. Modern Tunnel Technol 056(006):145–150

Pruitt E, Heng C, King J, Reed A, & Liu X (2022) An experimental study of the heat balance in a subsonic wind tunnel. In: AIAA SCITECH 2022 Forum (p. 0967)

Ren R, Xu S, Ren Z, Zhang S, Wang H, Wang X, He S (2018) Numerical investigation of particle concentration distribution characteristics in twin-tunnel complementary ventilation system. Math Probl Eng 2018(2018):1–13

Roh JS, Yang SS, Hong SR, Yoon MO (2008) An experimental study on the effect of ventilation velocity on burning rate in tunnel fires-heptane pool fire case. Build Environ 43(7):1225–1231

Wan H, Gao Z, Han J, Ji J, Ye M, Zhang Y (2019) A numerical study on smoke back-layering length and inlet air velocity of fires in an

inclined tunnel under natural ventilation with a vertical shaft. Int J Therm Sci 138:293–303

Wang YQ, Xie YL, Liu HZ, Ren R (2010) Physical model experiment on semi transverse ventilation air inlet and outlet of subsea tunnel. China J Highway Transp. 23(3):76

Wang YQ, Hu YJ, Deng M, Xia FY, Xie YL (2014) Complementary ventilation operational test in large longitudinal slope double-hole tunnel. J Traffic Transp Eng 2014(5):29–35

Wang YQ, Xia FY, Xie YL, Hu YJ (2014) Physical model experiment on complementary ventilation of extra-long highway tunnel. China J Highway Transp 27(6):84

Wang ZL, Zhu L, Guo XX, Pan XH, Zhou B, Yang J, Feng L (2019) Reduced-scale experimental and numerical study of fire in a hybrid ventilation system in a large underground subway depot with superstructures under fire scenario. Tunnel Undergr Space Technol 88:98–112

Wang Y, Han X, Zhou T, He Z, Tian F, Zheng Z et al (2019) Road tunnel axial fan performance in situ test: taking qinling zhongnan mountain highway tunnel as an example. Math Probl Eng 2019:1–12

Wang Y, Xu S, Ren R, Zhang S, Ren Z (2020) Application of the twin-tube complementary ventilation system in large-slopping road tunnels in China. Int J Ventil 19(1):63–82

Wang YD, Qin ZJ, He ZW, Wang W, Liu DX (2020) Improved mixed ventilation mode combined double-hole complementarity with blowing ang exhausting shaft in highway tunnel. China J Highway Transp. 33(004):106–114

Wang YD, Hua SH, He ZW, Qin ZJ, Wang W, Liu DX (2020) Mixed ventilation design system combined cross passage with single Shaft in extra-long highway tunnel. J Transport Eng 20(06):161–170

Xia FY, Wang YQ, & Xie YL (2015). Design method and test of twin-tunnel complementary ventilation for highway tunnel. J Highway Transport Res Dev. 32 3

Xie YY, Hu ZR, Lu GJ, Zhang XM, Lai KC (2013) Instant numerical simulation research on fire ventilation in extra-long highway tunnel in zhongnanshan section of qinlin mountains. Proc Eng 52(6):468–474

Zhang GP, Lei B, Tian ML (2011) Study on air interchange system for road tunnel longitudinal ventilation. Modern Tunnel Technol 48(1):42–45

Zhang Z, Zhang H, Tan Y, Yang H (2018) Natural wind utilization in the vertical Shaft of a super-long highway tunnel and its energy saving effect. Build Environ 145:140–152

Zhang GP, Lei B, & Lei ML (2011b). Application of air exchange method in longitudinal ventilation of highway tunnel. Modern Tunnel Technol, (01): 48-51+62

Zhou Y, Chen F, Chen J, Jiang B (2020) Influence of multisource fire on temperature distribution and natural smoke exhaust effect in urban tunnels with a shaft. Fire Mater 44:724–735